Chemically Reactive Flows in Aribag Inflator Chambers

Kyoung su Im, Grant Cook, Jr., and Zeng-Chan Zhang

Livermore Softwar Technoglogy Crop.

Abstract

Airbags are part of an important vehicle safety system, and the inflator is an essential part that generates a specific volume of gas to the airbag for a short duration of time. Recently, we have developed numerical models of automotive airbag inflators in conjunction with the LS-DYNA® chemistry solver. In this study, detailed and comprehensive descriptions for theoretical models are developed for a conventional pyrotechnic inflator (PI) and a compressed, heated gas inflator (HGI). For the model validation, the closed bomb test was executed and compared with an experimental data, In case of pyrotechnic inflator, zero dimensional model in conjunction with a solid propellant grains (e.g. NaN3/Fe2O3) is applied and the results are compared with existing data. In HGI model, a 2-dimensional with multi-species chemically reacting flow was calculated in the combustion chamber. Detailed and comprehensive descriptions for constructing the keyword flies will be given and the results for the two models will be discussed.

The present study should find wide applications in designing advanced inflator models and predicting airbag performance by coupling to LS-DYNA® airbag solvers (i. e., ALE/ CESE).

1 Introduction

The modeling zones of the pyrotechnic inflator generally consist of the propellant, combustion chamber, gas plenum, and discharge tank [1-3] as shown in Fig. 1a. Propellant grains including igniting material are contained and confined to the combustion chamber, which is completely sealed from the rest of the inflator by a thin rupture disk, so that the pressure of the combustion chamber is maintained until it reaches a desired value. With rapidly increasing pressure and temperature due to combusting propellant grains, the high pressure in the combustion chamber opens up the rupture disk to open. Then, the filter screen between the combustion chamber and the gas plenum captures the condensed phase slag and also cools the hot gas by permeating through the wide surface area heat sink. When the combustion gas fills in the gas plenum and the pressure in it exceeds a certain specified value, another rupture disk opens and the product gases exhaust into the discharge tank. Since the pressure, temperature and mass flow rate in the discharge tank caused by the performance of the inflator characteristics are the crucial factor in designing an airbag, the purpose of the simulation model is to provide accurate information concerning the combustion gas.

Recently, O'Loughlin et al. [4] published a U.S. patent for a heated gas inflator (HGI) that avoids several drawbacks for the conventional pyrotechnic inflator; 1) variable performance depending on the ambient condition, 2) disposal of un-burnt propellants, 3) toxicity of the combustion products. Figure 1b illustrates the schematic of the cross-sectional view of such inflators, which have cylindrical shapes and are initially filled to very high pressure with a gaseous mixture of fuel and oxidizer.

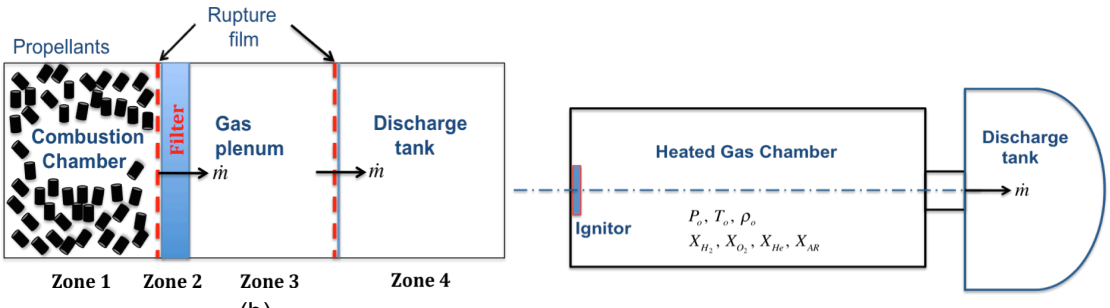

(b)

Figure 1 Schematic of the cross-section of pyrotechnic airbag inflator (a), and a typical passenger-side heated gas inflator for the simulation model.

The HGI consists of an igniter, pressurized initial mixture chamber, and the discharge tank including exit nozzle. The common fuel is hydrogen with oxygen and the diluting gases are typically helium, nitrogen and Argon. Initially, the canister chamber in the HGI is filled with pressurized fuel and mixture gases. By triggering with an electric signal, the igniter initiates the combustion, which propagates through the canister and eventually generates strong detonation waves in the downstream direction. Then, a rupture disk having the same purpose as in a pyrotechnic inflator breaks open and allows gas flow into the discharge tank or airbag.

2 Theoretical Models

2.1 Pyrotechnic Inflator"

The actual pyrotechnic inflator model is a complex problem since it contains a multi-phase and multi-component explosive reacting flow in the combustion chamber. As a result, the model is typically simplified to a zero-dimensional model, meaning that no momentum equations are considered, under various assumptions [1]. Based on the model assumptions, applying the mass and energy conservation principles to the model can derive the conservation equations for the pyrotechnic inflator. The species mass conservations equations are given as,

$$\frac{dm_{k,g,j}}{dt} = y_{k,g,j-1}\dot{m}_{g,j-1} - y_{k,g,j}\dot{m}_{g,j} + \psi_{k,g,j} \tag{1}$$
$$\frac{dm_{k,c,j}}{dt} = y_{k,c,j-1}\dot{m}_{c,j-1} - y_{k,c,j}\dot{m}_{c,j} + \psi_{k,c,j}$$

Here, index k and j indicate the species, and the zone number, respectively. The index g represents gas phase and c represents condensed phase. The m, t, y, $\dot{m}$, and ψ are the mass, time, mass fraction, mass flow rate and mass generation.

The gas phase and the condensed phase energy equations for each zone can be expressed as,

$$\begin{aligned} m_{g,j}c_{vg,j}\frac{dT_{g,j}}{dt} &= \dot{m}_{g,j-1}h_{g,j-1} - \dot{m}_{g,j}h_{g,j} + \dot{\omega}_{g,j}h_f + P_jV_j\frac{d\phi_j}{dt} + Q_{g,j} \\ &\quad - \sum_{k=1}^{N_g} e_k(T_g)\frac{dm_{k,g,j}}{dt} \\ m_{c,j}c_{vc,j}\frac{dT_{c,j}}{dt} &= \dot{m}_{c,j-1}h_{c,j-1} - \dot{m}_{c,j}h_{c,j} + \dot{\omega}_{c,j}h_f - P_jV_j\frac{d\phi_j}{dt} + Q_{c,j} \\ &\quad - \sum_{k=1}^{N_c} e_k(T_c)\frac{dm_{k,c,j}}{dt} \end{aligned} \tag{2}$$

where c_v is the specific heat, h the enthalpy, P the pressue, V_j the volume, T the temperature, φ the condensed phase volume fraction, and Q stands for heat transfer.

The constitutive relations used in Eq. (1) and (2) are the regression rate of the solid propellant grains, mass flow rate through the nozzles, condensed phase porosity, and an equation of state for the gas phase species. The mass generation term in Eq.(1) of the species k for the phase i in the each zone can be expressed as,

$$\psi_{k,i,j} = y_{k,i,p}\dot{\omega}_{i,j} \tag{3}$$
$$\text{with } \dot{\omega}_{i,j} = y_{g,p}\frac{dm_r}{dt}, \text{ and } \dot{\omega}_{i,j} = y_{c,p}\frac{dm_r}{dt}$$

Here, $y_{k,i,p}$ is the mass fraction of species k, which are evaluated relative to the products of combustion in phase i, and $\dot{\omega}_{i,j}$ is the mass production rate of phase i in the jth zone. Since the propellant combustion occurs in zone 1 only, the mass production rate can be restricted in the combustion chamber. The total mass generation term appeared in Eq. (3), and is expressed as,

$$\frac{dm_r}{dt} = N \cdot A_r(r)\rho_r\dot{r}_r \tag{4}$$

Here, N is the total number of propellant grains, Ar(r) is the instantaneous surface area of a grain, ρ is the propellant density and $\dot{r}$ is the steady state regression rate of the propellant, which is given as this empirical relation,

$$\dot{r}_r = aP^n$$

where n is an empirical constant determined by experiment. The power law coefficient is given by[1],

$$a = \begin{cases} 0 & t \le t_{delay} \\ a_0\dfrac{t - t_{delay}}{\Delta t} & t_{delay} < t \le t_{delay} + \Delta t_{rise} \\ a_0 & t \ge t_{delay} + \Delta t_{rise} \end{cases} \tag{5}$$

where a_0 is the steady-state value measured in experiment. The ignition delay time is taken to be the instants when the combustion temperature reaches an ignition temperature. The temperature rising time is due to the energy release of the ignitor unit in the combustion chamber.

Since the pyrotechnic model is zero-dimensional, the momentum equation is not considered as a governing equation. Thus, the mass flow rate exiting each nozzle must be determined from a gas dynamics law. The gas phase mass flow rate through the combustion chamber (zone 1) is given as,

$$\dot{m}_{g,1} = A_f c d_f \left\{ \frac{2\gamma}{\gamma-1} p_1 \rho_1 \left[\left(\frac{p_3}{p_1} \right)^{\frac{2}{\gamma}} - \left(\frac{p_3}{p_1} \right)^{\frac{\gamma-1}{\gamma}} \right] \right\}^{1/2} \tag{6}$$

Once the gas phase mass flow rate is determined, the condensed phase mass flow rate is calculated by assuming the following proportional relation,

$$\dot{m}_{c,1} = \dot{m}_{g,1} \left(\frac{m_{c,1}}{m_{g,1}} \right) \tag{7}$$

The gas phase mass flow rate exiting the inflator nozzle (zone 3) can also be determined by applying a gas dynamics law between the gas plenum and the discharge tank.

$$\dot{m}_{g,3} = A_n c d_n \left\{ \frac{2\gamma}{\gamma-1} p_3 \rho_3 \left[\left(\frac{p_4}{p_3} \right)^{\frac{2}{\gamma}} - \left(\frac{p_4}{p_3} \right)^{\frac{\gamma-1}{\gamma}} \right] \right\}^{1/2}, \text{ if } p_4 > p_{cr} \tag{8}$$

$$= A_n c d_n \sqrt{\gamma p_3 \rho_3} \left(\frac{2}{\gamma-1} \right)^{\frac{\gamma+1}{2(\gamma+1)}} \qquad \text{, if } p_4 \le p_{cr}$$

Here, the critical pressure is defined as,

$$p_{cr} = p_3 \left(\frac{2}{\gamma+1} \right)^{\frac{\gamma}{\gamma-1}} \tag{9}$$

Again, the condensed phase is given by the same principle.

$$\dot{m}_{c,3} = \dot{m}_{g,3} \left(\frac{m_{c,3}}{m_{g,3}} \right) \tag{10}$$

The condensed phase volume fraction and its derivative shown in the energy equation are given by [1],

$$\varphi_j = \frac{1}{V_j} \sum_k \frac{m_{k,c,j}}{\rho_{k,c}} \tag{11}$$

and its derivative,

$$\frac{d\varphi_j}{dt} = \frac{1}{V_j} \sum_k \frac{1}{\rho_{k,c}} \frac{dm_{k,c,j}}{d\rho_{k,c}} \tag{12}$$

where V_j is the volume of each zone. The condensed phase apparent density is determined as,

$$\rho_c = \frac{m_c}{V_c} = \frac{1}{\sum_k \frac{y_{k,c}}{\rho_{k,c}}} \tag{13}$$

The ideal gas equation of state is given as,

$$p = \rho R T \tag{14}$$

where the gas constant R is based on the local gas phase composition.

2.2 Heated Gas Inflator

The governing equations for the heated gas inflator are 2-dimensional multi-species reactive Euler equations, which can be given as,

$$\frac{\partial \vec{u}}{\partial t} + \frac{\partial F(\vec{u})}{\partial x} + \frac{\partial G(\vec{u})}{\partial y} = \alpha H(\vec{u}) + S(\vec{u}) \tag{15}$$

where

$$\vec{u} = \begin{bmatrix} \rho \\ \rho u \\ \rho v \\ \rho E_t \\ \rho y_1 \\ \vdots \\ \rho y_{N_s-1} \end{bmatrix}, F(\vec{u}) = \begin{bmatrix} \rho u \\ \rho u^2 + P \\ \rho uv \\ (\rho E_t + P)u \\ \rho u y_1 \\ \vdots \\ \rho u y_{N_s-1} \end{bmatrix}, \text{ and } G(\vec{u}) = \begin{bmatrix} \rho u \\ \rho uv \\ \rho v^2 + P \\ (\rho E_t + P)v \\ \rho v y_1 \\ \vdots \\ \rho v y_{N_s-1} \end{bmatrix}$$

are the main variable vector, x- and y-direction the flux vectors, respectively. The source terms due to geometries and combustion, respectively are given as,

$$H(\vec{u}) = -\frac{1}{y}\begin{bmatrix} \rho v \\ \rho uv \\ \rho v^2 \\ (\rho E_t + P)v \\ \rho v y_1 \\ \vdots \\ \rho v y_{N_s-1} \end{bmatrix}, \text{ and } S(\vec{u}) = \begin{bmatrix} 0 \\ 0 \\ 0 \\ 0 \\ \rho\Omega_1 \\ \vdots \\ \rho\Omega_{N_s-1} \end{bmatrix}$$

In the above, *u*, *v*, and are the velocities, ρ and *P* are the mixture density and pressure, x, y, and z are the distances, *t* is the time, y_k is the mass fraction of species *k*. E_t is the specific total energy per unit volume defined as,

$$E_t = e + \frac{1}{2}u_i \ , \quad (i = 1,2) \tag{16}$$

where *e* is the specific internal energy. Note that $\alpha = 0$ corresponds to the nominal 2-D flow, and $\alpha = 1$ to axi-symmetric flow.

Since the total mass of such a multi component mixture remains constant, the density is given by,

$$\rho = \sum_{k=1}^{N_s} \rho_k \tag{17}$$

as $y_k = \rho_k / \rho$, the summation of all species is given as,

$$\sum_{k=1}^{N_s} y_k = 1 \tag{18}$$

Ω_k is the production rate of species k , which is given by some kinetic rate law.

$$\Omega_k = \frac{M_k \dot{\omega}_k}{\rho} \tag{19}$$

where M_k is the molar mass of species k and $\dot{\omega}_k$ is the net molar production rate of species k . For a system of reacting ideal gas, calculation of $\dot{\omega}_k$ requires a detailed mechanism of elementary reactions. For a system of N_r elementary reactions involving N_s species, the rate equation can be written in the following general form,

$$\sum_{k=1}^{N_s} \nu'_{ki} X_k \Leftrightarrow \sum_{k=1}^{N_s} \nu''_{ki} X_k, \quad i = 1,\ldots,N_r \tag{20}$$

where ν'_{kl} and ν''_{kl} are the forward and backward stoichiometric coefficients respectively, X_k is the chemical symbol for the species *k*, and N_r is the total number of reactions in the mechanism. The net molar production rate of species *k* is given by,

$$\dot{\omega}_k = \sum_{i=1}^{N_r} \nu_{ki} q_i, \quad k = 1,\ldots,N_s \tag{21}$$

where $\nu_{ki} = \nu''_{ki} - \nu'_{ki}$, and

$$q_i = k_{fi} \prod_{k=1}^{N_s} [X_k]^{\nu'_{ki}} - k_{bi} \prod_{k=1}^{N_s} [X_k]^{\nu''_{ki}} \tag{22}$$

where k_{fi} and k_{bi} are the forward and backward rate coefficient of reaction *i*, and $[X_k] (= \rho_k / W_k, \text{ where } \rho_k \text{ is the species concentration})$ is the molar concentration of species *k*. The forward rate coefficient are typically expressed as,

$$k_{fi} = A_{fi} T^{\beta_{fi}} \exp\left(-\frac{E_{fi}}{RT}\right) \tag{23}$$

where A_{fi} is the pre-exponential factor, β_{fi} is the temperature exponent, E_{fi} is the activation energy per unit mole, *T* is temperature, and *R* is the universal gas constant.

For reactions provided with backward rate coefficients, the backward rate constants k_{bi} are computed in a similar fashion to the forward rate constant. However, if the backward coefficients are not specified, the backward rate constants are computed based on k_{fi} and the equilibrium constant K_{ci}.

$$k_{bi} = k_{fi} \Big/ K_{c_i} \tag{24}$$

The specific heat and enthalpy of the species can be evaluated using the JANAF Table polynomials.

$$\frac{C_{pk}^{o}}{R} = a_{1k} + a_{2k}T + a_{3k}T^2 + a_{4k}T^3 + a_{5k}T^4$$
$$\frac{H_{k}^{o}}{RT} = a_{1k} + \frac{a_{2k}}{2}T + \frac{a_{3k}}{3}T^2 + \frac{a_{4k}}{4}T^3 + \frac{a_{5k}}{5}T^4 + \frac{a_{6k}}{T} \quad (25)$$

The coefficients of these polynomials expansions which are valid in a temperature range 200K to 6000K are supplied by Gordon and McBride [5].

3 Results and Discussion

The numerical analysis and an experiment were carried out for a closed bomb test (CBT), with the chemistry model validation using 40 g of Tritonal propellant charge. The CBT chamber has a dimension of 40 cm in radius (r; y, z) and 150cm in longitudinal length, so that the total volume of the chamber is 0.754 m^3. Two pressure gauges (Kulite; HEL-375-250A, and HEL-375-500A) having different sensing capacities were installed, the one at the front center of the cylinder (x=750 cm, r= 40 cm) and the other at the side center of the cylinder base surface (x=150 cm, r= 0 cm), respectively. Figure 2 shows the CBT validations with the pressure data sets for the side and front center position between the simulation results and averaged experimental data. Figure 2(a) and (b) illustrate the pressure history at the side and front center, respectively.

It is clear that the simulation results are in excellent agreement with the experimental data over the time ranges.

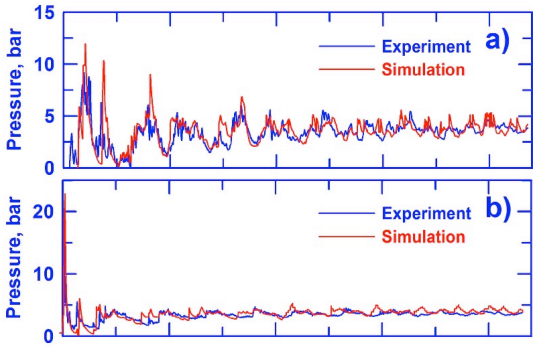

Figure 2 Comparisons between measured data and simulation at the side and front center positions: a) and b) are the pressure histories.

Since the total mass generation of the propellant is given by Eq. (4), the mass amounts of product species for the solid propellants combustion are assumed to be proportion to the species mass fractions, which are determined by a thermochemical equilibrium code [5]. However, the mass fractions of principal species account for over 99 percent of the total, indicating that minor species can be neglected. Thus, for simplicity, a stoichiometric reaction is used for the reactants and products as,

$$6NaN_3(s) + Fe_2O_3(s) \rightarrow 2Fe(s) + 3Na_2O(s) + 9N_2 \quad (26)$$

All input data for the simulation were chosen to be the same as reference [1]

Figure 3 shows the temperature profiles in the combustion chamber and gas plenum. Due to the initial energy release from the igniter and propellants, the temperature increases quickly. When the interior rupture film on the combustion chamber wall breaks, gas and condensed phase species flow from the combustion chamber to gas plenum, resulting in an increased the temperature in the gas plenum. Initially, due to existing the N2 and O2 gases at standard conditions in gas plenum, the maximum temperature of the gas plenum is a little higher than that in the combustion chamber.

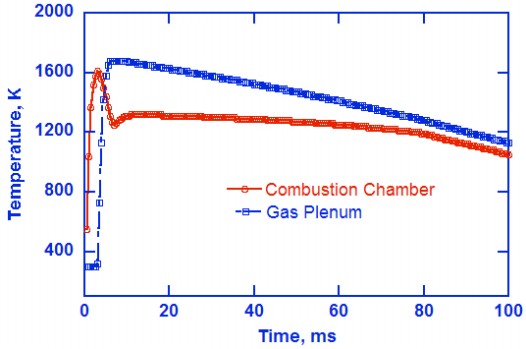

Figure 3 Temperature profiles in the combustion chamber and gas plenum with time.

Figure 4 shows the pressure profiles both in the combustion chamber and the gas plenum. Due to the rapid energy release from the solid propellants, high pressure breaks the interior rupture film. Thus, a certain amount of gas flows into the gas plenum. Due to the sudden discharge of gas, the pressure in the combustion chamber shows a sharp decrease as can be seen in the temperature profile in Fig. 3. After this, a steady-state combustion mode is reached for the remaining period of time. Again, due to the initial condition in the gas plenum, the maximum pressure and the curve profile are similar to that in the combustion chamber.

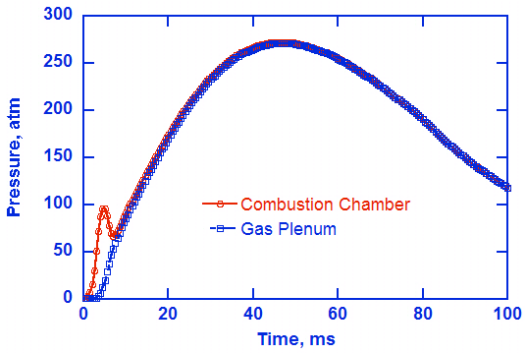

Figure 4 Pressure profiles in the combustion chamber and gas plenum with time.

Figure 5 shows the typical thermodynamics properties such as the density, pressure, and temperature as a function of time in the discharge tank in the pyrotechnic inflator simulation. With an initial delay time after which the gas flow arrives at the discharge tank, all variables are moderately increased until reaching their convergence values. The maximum pressure is about 1.6 atm and the corresponding temperature is approximately 400K, which is suitable for the airbag deployment process.

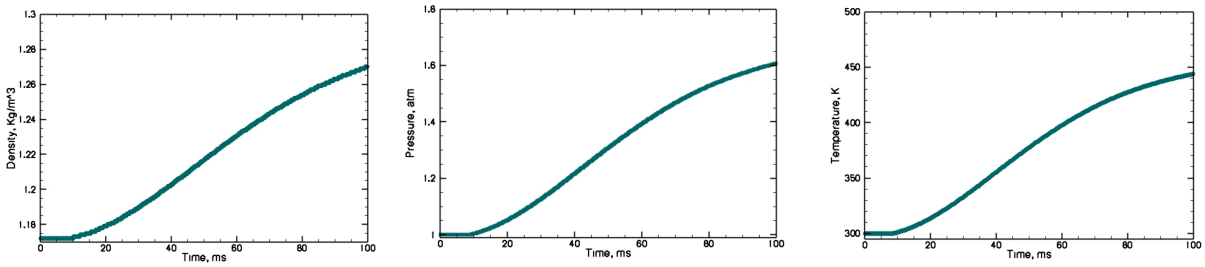

(a) (b) (c)

Figure 5 Thermodynamics properties at the discharge tank (zone 4) for the pyrotechnic inflator: (a) density, (b) pressure, and c) temperature

4 Summary

In this study, we have demonstrated the performance of two different inflator models: a conventional pyrotechnic inflator and a compressed, heated gas inflator. Detailed and comprehensive descriptions of theoretical and mathematical models are provided. For the model validation purpose, the results between the numerical simulation and an experimental data set were compared, showing excellent agreement. With the development of these validated inflator models, we strongly believe that the present work should find more applications in designing advanced inflator models and predicting airbag performance.

5 Refoerences

[1] Butler, P. B., Kang, J., and Krier, H., *Prog. Energy Combust. Sci., 19*:365-382 (1993).
[2] Schmitt, R. G., Butler, P. B., and Jon, J. F., *Combustion Sci. and Tech.*, 122:1-6, 305-330 (1997).
[3] Seo, Y.-D. Chung. S. H., and Yoh, J. J., *Fuel, doi:10.1016/j.fuel.2010.12.042* (2011).
[4] O'Loughlin, J. P.and Stevens H. O., " Heated Gas Inflator,", US Patent0290108 (2006).
[5] Gordon, S. McBride, B.J, "Computer Program for Calculation of Complex Chemical Equilibrium Compositions, Rocket Performance, Incident and Reflected Shocks, and Chapman-Jouguet Detonations," NSSA SP-273 (1976)